Hybrid-activated carbon electrodes decorated with different transition metals for supercapacitor applications

Vanzetto, Andrielen Braz; Teloken, Francisco; Beltrami, Mateus; Lazzari, Lidia Kunz; Júnior, Heitor Luiz Ornaghi; Monticeli, Francisco Maciel; Poletto, Matheus; Dias, Otávio Titton; Zattera, Ademir José

DOI
10.1016/j.diamond.2025.112688

Publication date
2025

Document Version
Final published version

Published in
Diamond and Related Materials

Diamond & Related Materials 158 (2025) 112688

Contents lists available at ScienceDirect

Diamond & Related Materials

journal homepage: www.elsevier.com/locate/diamond

Hybrid-activated carbon electrodes decorated with different transition metals for supercapacitor applications

Andrielen Braz Vanzetto [a], Francisco Teloken [a], Mateus Beltrami [b], Lidia Kunz Lazzari [a], Heitor Luiz Ornaghi Júnior [a,*], Francisco Maciel Monticeli [c], Matheus Poletto [a], Otávio Titton Dias [d], Ademir José Zattera [a]

[a] Postgraduate Program in Engineering of Processes and Technologies (PGEPROTEC), University of Caxias do Sul (UCS), R. Francisco Getúlio Vargas, 1130, 95070-560 Caxias do Sul, RS, Brazil
[b] Postgraduate Program in Mining, Metallurgical and Materials Engineering, Federal University of Rio Grande do Sul (UFRGS), Porto Alegre, Brazil
[c] Department of Aerospace Structures and Materials, Faculty of Aerospace Engineering, Delft University of Technology, 2629, HS, Delft, the Netherlands
[d] Centre for Biocomposites and Biomaterials Processing, Department of Mechanical and Industrial Engineering, Faculty of Applied Science and Engineering, University of Toronto, 5 King's College Road, Toronto, Ontario M5S 3G8, Canada

ARTICLE INFO

Keywords:
Energy storage
Supercapacitors
Carbon electrodes
Metal-decorated carbon

ABSTRACT

This research investigated the combination of acid functionalization and metal deposition on commercial activated carbon (AC) for the synthesis of electrodes for applications in supercapacitors. The effect of acid treatment and the deposition of metals, including nickel, copper, and cobalt on the electrochemical characteristics of the carbon material were assessed. The AC treatment with sulfuric acid resulted in a nearly twofold increase in surface area compared to the untreated AC, enhancing porosity and creating irregularities that improved the motion of ions and electrons, increasing the specific capacitance and energy density. Notably, we demonstrate that nickel deposition at only 2 wt% significantly improved specific capacitance (up to 59.58 $F{\cdot}g^{-1}$), while preserving porosity and enhancing surface wettability. The adoption of a scalable, solvent-free, and low-energy technique for metal deposition on carbon structures presents promising opportunities for developing sustainable alternatives in energy storage technologies.

1. Introduction

The growing interest on renewable energy sources, including wind and solar, requires the development of efficient energy storage systems due to the intermittent and seasonal nature of power generation. Among the storage technologies, supercapacitors have emerged as promising candidates, offering high power densities, rapid charge–discharge cycles, and long-term stability [1–3].

Carbon-based materials have attracted widespread attention for supercapacitor electrodes due to their high surface area, structural stability, and availability from biomass or agro-industrial residues [2,4,5]. In particular, activated carbon (AC) stands out for its tunable porosity and cost-effectiveness. However, commercial AC often requires surface modification to enhance its electrochemical properties, including specific capacitance and wettability. Strategies such as acid or base treatments have been used to increase surface area and introduce functional groups that promote ion transport and electrolyte compatibility [5,6].

Some recent studies show different methodologies for the production of supercapacitors with AC. For example, the study carried out by Vega-Ramirez et al. (2025) [7] in which N,P-doped carbon materials were produced from a chemical treatment of chitosan with H_3PO_4, followed by thermal treatment, and obtaining Chitosan-derived activated carbon with a surface area of 1515 $m^2{\cdot}g^{-1}$ and unique electrochemical properties. Polyaniline (PANI) was electrochemically polymerized onto the surface of human hair–derived activated carbon (HH-AC) coated on a nickel foam substrate using cyclic voltammetry (CV) with varying numbers of cycles. Unlike conventional electrochemical polymerization methods, the bilayer HH-AC/PANI electrode was synthesized in a non-acidic medium. The optimized electrode, obtained after 8 CV cycles and designated as HH-AC/PANI-8, exhibited an excellent specific capacitance of 220 $F{\cdot}g^{-1}$ at a positive potential [8]. Some other technologies used recently were, carbon retrieved from the rice husk and its combination with binary transition metal sulfides (ZnS/FeS) [9], sulfur-doped apricot shell activated carbons (S-ASAC) [10], lentil processing

* Corresponding author.
E-mail addresses: ornaghijr.heitor@gmail.com (H.L.O. Júnior), f.m.monticeli@tudelft.nl (F.M. Monticeli).

https://doi.org/10.1016/j.diamond.2025.112688
Received 4 June 2025; Received in revised form 15 July 2025; Accepted 29 July 2025
Available online 31 July 2025

residual (LPR) in the form of microwave-supported activated carbon (LPRAC) [11], between others. Another effective route to improve AC performance is metal doping, particularly with transition metals like cobalt, copper, and nickel, which contribute to pseudocapacitance through Faradaic reactions [4,12,13]. These metals also promote surface conductivity and redox activity. Studies have shown that combining metal species with carbon structures can significantly enhance energy and power density in supercapacitors [14–16]. Various methods have been explored for metal incorporation, including wet impregnation, hydrothermal synthesis, and electrochemical deposition [17]. However, many of these techniques suffer from issues such as high energy consumption, solvent use, or limited control over film uniformity. Magnetron sputtering has gained attention as a solvent-free and scalable alternative for depositing uniform metal films on porous carbon substrates, with the added benefit of preserving the material's structural integrity [18,19]. Yet, the use of sputtering for decorating chemically treated commercial AC remains underexplored. Based on literature insights, nickel, cobalt, and copper were selected due to their widely reported electrochemical activity, conductivity, and catalytic potential in hybrid electrodes [4,15,20]. These metals also vary in terms of redox behavior and surface interaction with the carbon matrix, allowing for comparative analysis.

In this study, we investigate the effect of combining sulfuric acid treatment and magnetron sputtering deposition of transition metals (Ni, Cu, Co) on commercial activated carbon. The structural, chemical, and electrochemical properties of the modified electrodes were characterized to assess their performance in supercapacitor applications. Special attention was given to surface area, pore distribution, wettability, and specific capacitance. The novelty of this work lies in the synergistic dual-modification approach, which integrates mild chemical activation and precise solvent-free metal deposition. This strategy enables the development of high-performance, scalable, and sustainable carbon-based electrodes. To the best of our knowledge, this is the first study to systematically explore this combination on commercial AC, establishing clear correlations between physicochemical properties and electrochemical performance.

2. Materials and methods

2.1. Chemical treatment of commercial activated carbon

Commercial activated carbon (CAS: 7440-44-0, Kinetics Reagents and Solutions) was treated with sulfuric acid (purity ≥98 %, VETEC) following a methodology described in the literature for surface modification of activated carbon [21]. A ratio of 0.1:100 was used, corresponding to 0.1 g of activated carbon per 100 mL of 20 mmol·L^{-1} sulfuric acid solution, with stirring for 6 h. The samples were designated as AC-S, representing activated carbon treated with sulfuric acid. Following the acid treatment, the samples were washed with deionized water until a pH of approximately 5.8 was reached, then dried in an oven at 100 °C for 12 h.

2.2. Synthesis of electrodes

Metals were deposited on the acid-treated activated carbon surfaces using magnetron sputtering [22]. Cobalt (Co), Nickel (Ni), and Copper (Cu) were deposited at a concentration of 2.0 % (*w*/w), and the resulting samples were labeled AC-S2%Co, AC-S2%Ni, and AC-S2%Cu, respectively. The sputtering parameters included currents ranging from 150 to 400 mA, working pressures of 1.80 × 10^{-2} to 8.6 × 10^{-6} mbar, and deposition times from 1 to 40 min, depending on the sample.

Electrodes were fabricated using the slurry method, which involved forming a homogeneous paste from the active material, polymer, and fillers, applied to a substrate and dried. The component proportions followed the literature [23], with a 1:1:8 ratio of active material (AC + metal), polymer, and fillers. Polyvinylidene fluoride (PVDF) was used as the polymer, and commercial carbon black served as the filler. The slurry was applied to aluminum foil and dried to evaporate the solvent. Electrode samples measuring approximately 2 × 2 cm were prepared for characterization.

2.3. Characterization

The textural properties, surface area, total pore volume, and pore size distribution of the biocarbon samples were determined using the nitrogen adsorption/desorption method at −196 °C (77 K) with a Quantachrome Instruments (NOVA 1200e). The surface area and total pore volume were calculated from the adsorption/desorption isotherms using the BET (Brunauer, Emmet, and Teller) method, considering relative pressures in the range of P/P_0 = 0.05–1.0. The samples were initially subjected to a preparation procedure (degassing) to remove interfering agents present on the surface of the solid under analysis. This procedure was carried out under N_2 flow at a temperature of 200 °C for 20 h. The pore size distribution was calculated using the DFT (Density Functional Theory) function.

The morphology of the samples was visualized using field emission scanning electron microscopy (FEG-SEM), and images were obtained with a MIRA 3 microscope (TESCAN). Energy-dispersive X-ray spectroscopy (EDS) was employed to evaluate the presence and distribution of metals on the surface of the activated carbon.

The surface chemistry was investigated by X-ray photoelectron spectroscopy (XPS) using a monochromatic Al Kα X-ray source operated at 15 kV and 10 mA. The pass energy for the survey scan and element scan was set to 100 eV and 50 eV, respectively, with step sizes of 1 eV and 0.1 eV.

For electrochemical characterization, cyclic voltammetry (CV) tests were performed using an Ivium potentiostat, a Hg_2Cl_2 reference electrode, and a platinum counter electrode. The analysis parameters included scan rates of 30, 50, 100, 150, 200, and 250 mV s^{-1}, with a step size of 10 mV and a voltage range of −0.2 V to 1 V. The electrolyte used was a 1 M aqueous solution of Na_2SO_4.

To determine the specific capacitance values (C_s) of the electrodes, Eq. (1) was applied to each CV analysis, considering the mass (m, in grams), scan rate (v, in volts per second), potential difference (ΔV, in volts), electric current (I, in amperes), and specific capacitance (C_s, in farads per gram):

$$Cs = \frac{1}{m\nu\,\Delta V}\int_{Vi}^{Vf} I(V).dV \tag{1}$$

From the specific capacitance it is possible to calculate the energy density using Eq. (2), where E (Wh kg^{-1}) is the energy density, Cs is the specific capacitance derived from CV curves given by $F.g^{-1}$ and V is the operating voltage (V):

$$E = \frac{1}{2}.CsV^2.\left(\frac{1000}{3600}\right) \tag{2}$$

Galvanostatic charge-discharge (GCD) measurements were conducted to monitor the potential of the system as a function of time under the application of a constant current. The power density was determined using Eq. (3), P (W kg^{-1}) is the power density, E (Wh kg^{-1}) is the energy density and Δt (h) is the discharge time given by Eq. (40:

$$P = \frac{E}{\Delta t}.3600 \tag{3}$$

$$\Delta t = \frac{2\Delta V}{\nu} \tag{4}$$

GCD experiments were performed using a Swagelok-type test cell in a symmetric configuration, with a cellulose separator and Na_2SO_4 as the electrolyte. A current of 10 mA was applied, and 600 charge-discharge cycles were evaluated. All electrochemical tests used samples with the same useful area (0.075 cm^2) for comparison purposes. Electrochemical

impedance spectroscopy (EIS) was conducted from 100 mHz to 10 kHz using the same cell configuration as cyclic voltammetry.

The wettability of the electrode material was investigated by measuring the contact angle with water. These measurements were performed in triplicate at room temperature, at time $t = 0$ s.

3. Results and discussion

3.1. Acid treatment

Micrographs in Fig. 1 show the surface appearance of (a) commercial activated carbon (AC) and (b) sulfuric acid-treated activated carbon (AC-S). The micrographs reveal large clusters of particles distributed irregularly across the surface of AC-S, confirming the increased surface area observed via BET method. Energy-dispersive spectroscopy (EDS) analysis (Fig. S.1) confirmed the presence of sulfur on the AC-S surface, though quantification was not possible.

Table 1 presents the surface area analysis results obtained using BET method. The chemical surface treatment with sulfuric acid increased the surface area of AC by over 86 % (from 562 to 1.048 $m^2.g^{-1}$), attributed to a reduction in pore diameter and a higher total pore volume. Micro and mesopore were identified after acid treatment. Micropores and mesopores are essential for effective ion transport and charge storage. Micropores facilitate high capacitance, while mesopores support ion movement and increases power density. A larger pore volume allows greater ion accommodation, which contributes to an increase in the capacitance. Surface functionalization can improve wettability and electrode-electrolyte interactions by increasing the effective area and reducing ion transference resistance [24].

This simple methodology, employing low acid concentrations without exposing activated carbon to high temperatures, achieved a surface area approximately 60 % greater than the 680 $m^2.g^{-1}$ reported by Abdelouahab-Reddam et al. [25] for commercial activated carbon treated with H_2SO_4 under more intense conditions.

The physicochemical properties of activated carbon (AC), such as specific surface area, pore size distribution, and surface functional groups are strongly influenced by the synthesis route, particularly the type of activating agent, temperature, and atmosphere used during carbonization and activation processes. For instance, chemical activation with acids or bases can promote the formation of micro- and mesopores, while high-temperature treatments generally favor pore widening and graphitization [5,6,26]. According to Heidarinejad et al. [21], activation temperature and precursor characteristics directly affect the development of surface area and functional group density, which determines electrolyte accessibility and capacitance behavior. Yakout and Sharaf El-Deen [5] also emphasize that the nature of the activating agent (e.g., H_3PO_4 vs. KOH) plays a crucial role in tailoring the pore structure and surface chemistry. Teimouri et al. [27] highlight the importance of optimizing these parameters to align the carbon material's structure with the target electrochemical application. Although in the present study a commercial AC was used as the base material, the applied acid treatment and metal sputtering were sufficient to significantly enhance its surface area and wettability, demonstrating that even post-synthesis surface modifications can substantially improve electrochemical performance.

Type I and IV isotherm curves are typical of acid-treated activated carbons [28]. The nitrogen adsorption and desorption isotherms for AC-S (Fig. 2a) exhibited a type IV curve with a hysteresis loop between 0.2 and 1.0 P/P_o, indicating mesopore formation in the carbon texture. This is confirmed by evaluating the pore distribution curve as a function of pore volume (Fig. 2b), where a predominance of pores in the range of 50 to 200 Å is observed. Mesopores play an important role when larger electrolyte ions are used at increased working voltages, improving energy storage capacity [27]. Authors such as Demiral et al. [26], Yakout and Sharaf El-Deen [5], and Abdelouahab-Reddam et al. [25] also identified the predominance of mesopores in activated carbons treated with acids.

3.2. Metal deposition

Fig. 1c–e shows the FEG-SEM micrographs of the AC-S2%Co sample, where it is possible to observe the activated carbon particle coated with the metal oxide, forming a relatively uniform film (Fig. 1c and d), although cracks and peeling are visible in some regions (Fig. 1e).

In the micrographs of the AC-S2%Cu sample (Fig. 1f and g), exposed AC surfaces and irregularly scattered agglomerates are observed throughout the AC surface. In Fig. 1h, bright agglomerated and spherical spots can be seen, demonstrating the presence of the metal on the AC surface, as corroborated by the EDS analysis presented in Fig. S.2b. This morphological pattern is also observed by Tanapongpisit et al. [19]. In general, the coating by the sputtering method was satisfactory for this application. Further details on the influence of sputtering parameters on coating uniformity and electrode performance are provided in the Supplementary Material (Supplementary Note 1). The deposition of metals on the activated carbon samples was corroborated by EDS analysis (Fig. S.2), which indicated the presence of Co, Cu, and Ni metals on the surface of the AC-S. The presence of oxygen and sulfur, resulting from the acid treatment, stands out. Some metals, such as Al and Si, are present in the composition of the activated carbon used as the raw material.

Table 2 contains the results obtained from the N_2 sorption/desorption analysis for the samples of commercial activated carbon modified with sulfur acid containing metals. It was found that there was an increase in the surface area BET value from 1048 $m^2.g^{-1}$ of AC-S to 1432, 1984 and 1576 $m^2.g^{-1}$, for the AC-S2%Co, AC-S2%Ni and AC-S2%Cu samples, respectively. According to SEM-FEG micrographs in Fig. 1, the increase in the surface area can be attributed to a greater surface irregularity after the deposition of the metals by sputtering. Different morphologies of the deposited metal can be observed. In general, the metal particles cover the activated carbon in the form of a thin film (> 1 μm) with certain discontinuities (Fig. 1e). The morphology of the AC-S2%Cu sample stands out, where a characteristic aspect of the formation of CuO nanocrystals is observed (Fig. 1h) [20]. For the AC-S2%Ni sample (Fig. 1i–l), a more uniform coating is observed, without discontinuities (visible at this magnification). This result may be responsible for the formation of an electrical percolation network that will lead to better electrochemical results, as will be discussed below [29].

3.3. Surface chemistry

The incorporation of Ni, Cu, and Co into the AC-S matrix was confirmed by the increase in surface area observed in Tables 1 and 2, along with the proportional enhancement in the O 1s signal, associated with pore expansion during both the chemical solution and PVD sputtering processes and by the relative distribution of surface functional groups identified via XPS deconvolution of the C 1s and O 1s regions, as illustrated in Fig. 3.

This analysis demonstrates that the AC-S2%Ni sample exhibited the highest relative proportions of the C–OH/C–O–C functional group, both in the deconvoluted C 1s region (~286.3 eV; Fig. 3a) and O 1s region (~532.5 eV; Fig. 3b). This result suggests that, even at a low metal deposition concentration (2 %), the nickel doping process was sufficient to promote an oxygen-functionalized surface, rich in polar groups capable of interacting with the electrolyte [30].

Although the AC-S2%Ni sample exhibited the lowest relative content of graphitic carbon (C=C: 48.69 %, Fig. 3a) among the doped materials, its combination with higher proportions of oxygenated functional groups, such as C–OH/C–O–C (18.21 %, Fig. 3a) and C=O (16.17 %, Fig. 3a), resulted in a more balanced surface composition. In the O 1s region, this trend was also evident, with C–OH/C–O–C reaching 76.93 % (Fig. 3b), the highest among all samples. This chemical configuration may simultaneously support both efficient electron transport and

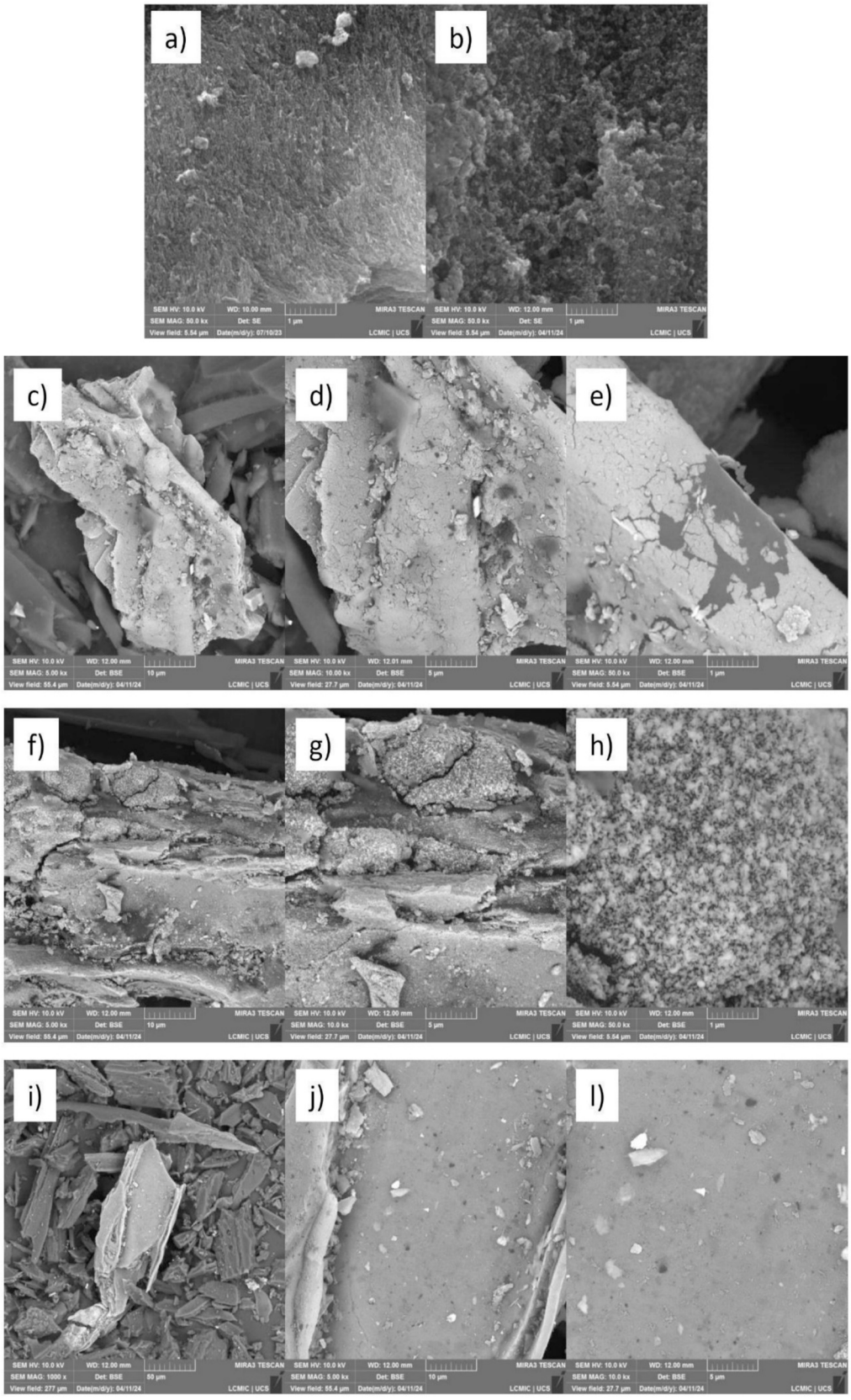

Fig. 1. FEG-SEM micrographs of the surface of (a) AC, (b) AC-S, (c–e) AC-S2%Co, (f–i) AC-S2%Cu, and (j–l) AC-S2%Ni.

Table 1
Surface analysis results using BET method for commercial activated carbon and sulfuric acid-treated carbon.

Sample	Surface area ($m^2\ g^{-1}$)	Pore Volume ($cm^3\ g^{-1}$)	Pore Diameter (nm)	Micropore volume ($cm^3\ g^{-1}$)	Mesopore Volume ($cm^3\ g^{-1}$)
AC	562.00	0.70	2.28	–	–
AC-S	1048.00	1.43	2.00	0.17	1.25

Faradaic charge storage at the electrode–electrolyte interface. The AC-S2%Co sample exhibited a slightly higher C–OH/C–O–C contribution in C 1 s (20.55 %), but a lower C═O proportion (15.96 %), while the AC-S2%Cu sample presented the highest graphitic content (C=C: 48.47 %) but the lowest C–OH/C–O–C (19.62 %) and C═O (15.96 %) fractions. Therefore, the relatively intermediate distribution of these components in the AC-S2%Ni surface may have favored its enhanced electrochemical performance. This interpretation is supported by literature reports in which nickel is shown to promote surface restructuring and chemical activation of carbon materials [30].

To investigate the chemical functionalities introduced by metal doping, Fig. 4 presents the high-resolution XPS spectra of the C 1 s and O 1 s regions for the electrodes AC-S, AC-S2%Co, AC-S2%Cu, and AC-S2%Ni. The deconvoluted C 1 s spectra (Fig. 4a–d) exhibit characteristic peaks assigned to graphitic carbon (C═C, ~284.4 eV), hydroxyl and ether functionalities (C–OH/C–O–C, ~286.3 eV), carbonyl groups (C═O, ~288.4 eV), and carboxylic functionalities (O–C=O, ~289.7 eV). Additionally, π–π* interactions are identified around ~291.5 eV. Similarly, the O 1s spectra (Fig. 4e–h) confirm the predominance of phenol and ether groups (C–OH/C–O–C, ~532.5 eV), alongside additional oxygen-containing species such as carbonyl (C═O, ~530.0 eV), carboxyl (O–C=O, ~535.0 eV), and metal oxide-related groups (~538.0 eV) [3].

Quantitative analysis of the XPS results (Fig. 3a and b) indicates that the AC-S2%Ni electrode exhibits a higher proportion of C–OH/C–O–C groups in both the C 1s (18.21 %) and O 1 s (76.93 %) regions compared to the other electrodes. Despite presenting a slightly reduced content of graphitic carbon (C═C, 48.69 %) relative to AC-S (54.17 %) and AC-S2%Cu (48.47 %), the AC-S2%Ni electrode demonstrates a balanced combination of oxygenated functionalities and conductive graphitic domains. This balance may enhance electrolyte wettability and facilitate efficient ion transport at the electrode-electrolyte interface. These oxygenated species, when combined with a moderately graphitized framework, are known to enhance both electric double-layer capacitance (EDLC) and pseudocapacitive storage, thus significantly contributing to the overall electrochemical performance and cycling stability in carbon-based electrode materials [31]. This enhanced electrochemical behavior correlates directly with structural modifications identified by BET analysis (Tables 1 and 2), particularly through the increased surface area and improved pore accessibility.

The enhanced electrochemical performance observed in the Ni-decorated activated carbon can be attributed to a synergistic effect between the oxygenated functional groups and the graphitic domains present on the electrode surface. The XPS analysis revealed a significant increase in C–OH/C–O–C and C═O functionalities, especially for the AC-S2%Ni sample, which contribute to improved pseudocapacitive behavior through fast and reversible Faradaic redox reactions at the electrode–electrolyte interface [30,31]. These polar groups also enhance electrolyte wettability, facilitating ion diffusion and increasing the electrochemically active surface area [3,32]. Also, the presence of graphitic carbon (C=C), although slightly reduced, ensures good electrical conductivity, which is essential for efficient charge transport across the electrode matrix [12,33]. The combination of these features promotes a balanced mechanism involving both electric double-layer capacitance (EDLC) and pseudocapacitance, resulting in improved specific capacitance and stability during cycling. Similar trends have been reported in studies using Ni or NiO-doped carbon materials, where increased oxygen functionality correlated with higher capacitance and improved cyclability [4,15,34]. However, the method adopted in this work, based on low-temperature acid treatment and solvent-free metal deposition via sputtering, offers a more sustainable and scalable

Table 2
Surface analysis results using the BET method for sulfuric acid-treated carbon with metals.

Sample	Surface area (m^2g^{-1})	Pore volume (cm^3g^{-1})	Pore diameter (nm)	Micropore volume (cm^3g^{-1})	Mesopore volume (cm^3g^{-1})
AC-S2% Co	1432	1.100	3.260	0.442	0.658
AC-S2% Ni	1984	1.519	3.256	0.626	0.893
AC-S2% Cu	1576	1.206	3.248	0.501	0.704

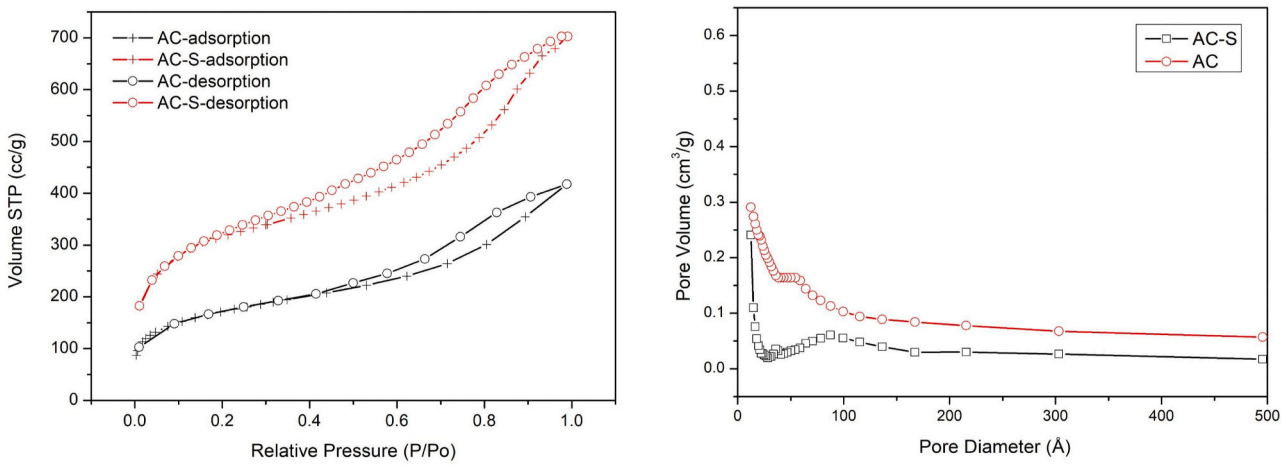

a) b)

Fig. 2. (a) N_2 adsorption-desorption curves and (b) pore diameter distribution for AC and AC-S.

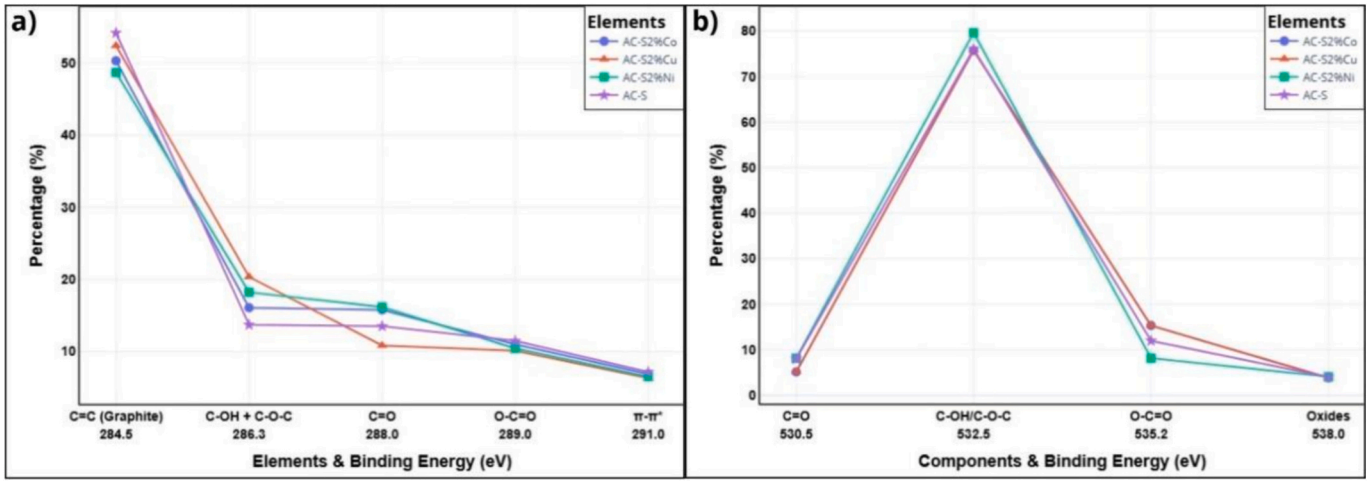

Fig. 3. Relative elemental area of contents of samples: a) C 1s, b) O 1s.

alternative, with comparable or superior performance to traditional wet chemical or hydrothermal synthesis routes.

3.4. Electrochemical characterization

3.4.1. Cyclic voltammetry

From the cyclic voltammetry curves of the produced electrodes, the specific capacitance of each sample was obtained, as shown in Table 3. The representative curves for each sample are presented in Fig. 5. It can be observed that, in general, the curves predominantly exhibited pseudocapacitive behavior, which is characteristic of activated carbon decorated with metals [12]. The specific capacitance is a parameter influenced by aspects of the porous material, such as the accessibility of the pores by the electrolyte, which can, in turn, be affected by surface chemistry, pore size, distribution, and orientation, among other factors [2].

It was found that the samples with the highest capacitance, when measured at a scan rate of 100 $mV{\cdot}s^{-1}$, were those containing 2 % Ni, showing a specific capacitance of 59.58 $F{\cdot}g^{-1}$. For cobalt and copper, the specific capacitance results were 29.40 and 30.47 $F{\cdot}g^{-1}$, respectively. According to Mandal et al. [17], activated carbon supercapacitors show good power density and cyclability, but low specific capacitance and energy density. Transition metal oxides have high specific capacitance but low cyclability. Transition metal oxides can be used to provide more Faradaic charge interaction methods to increase the performance of these activated carbon supercapacitors. However, the combined benefits of these individual components remain a challenge. According to the authors, there is an imbalance between the charge storage behavior of the two materials: the redox activity of the pseudocapacitive material and the conductivity of carbonaceous materials. A high amount of metal oxides could block the ion transport pathways inside the activated carbon matrix, while a low loading density would be insufficient.

For the sample that demonstrated higher specific capacitance, cyclic voltammetry measurements were performed at higher scan rates (Fig. 5) to verify the stability of the electrode, which is evidenced by the increase in the area of the curve. As previously mentioned, specific capacitance depends on different parameters and characteristics of the material and the synthesis process. The high specific capacitance value for the sample with 2 % Ni, 59.58 $F{\cdot}g^{-1}$, is also noteworthy. Other authors have also reported the use of Ni as a good material for composite electrodes with activated carbon for supercapacitors, finding specific capacitance values of similar magnitude [4,35].

In the comparison for different scan rates, the increase in curve area directly reflects the behavior of the electrode because the reaction predominates in the surface region, directly increasing the electric current drained during conduction. With the decrease in the time for deeper oxidation-reduction, the electrolyte ions are not completely diffused into the material, thus contributing to an increase in the area of cyclic voltammetry analysis. In relation to the other metals, the presence of copper demonstrated a less rectangular profile in the cyclic voltammetry. For some scan rates, a subtle shoulder may be perceived, indicating the occurrence of oxidation-reduction reactions and the existence of Faradaic capacitance in addition to typical double-layer capacitance [36,37].

Table 4 summarizes the specific capacitance values reported for various activated carbon-based materials modified by different activation methods and doping strategies. When compared to other studies, the Ni-modified commercial activated carbon developed in this work presented a moderate specific capacitance (59.58 $F{\cdot}g^{-1}$), yet with important advantages in terms of process simplicity, sustainability, and scalability, owing to the use of low-temperature acid treatment and solvent-free sputtering. While some studies report higher capacitance values—for instance, 249 $F{\cdot}g^{-1}$ for H_3PO_4-treated AC [41] or 364 $F{\cdot}g^{-1}$ for NiO/AC composites obtained via hydrothermal synthesis [42], these typically involve more complex, energy-intensive or multi-step methods, which may limit their industrial applicability.

3.4.2. Galvanostatic charge and discharge

Fig. 6 shows the GCD curves for all AC-S samples. In Fig. 6(a), a cycle of charge-discharge can be observed in the time interval between 1.2 s and 2.4 s. The plots for all samples resemble the typical triangular shape, indicating good double-layer behavior. A partially linear profile is observed for all samples, with the maximum peak load at 1.8 s, reaching E_{max} values of 2.18 V for AC-S, 2.07 V for AC-S2%Co, 1.94 V for AC-S2% Ni, and 1.90 V for AC-S2%Cu, respectively. After 600 cycles (Fig. 6(b)), the samples containing Ni and Cu showed no reduction in the maximum voltage reached during the charge cycle. Samples containing Co demonstrated a 0.2 V reduction in the maximum voltage during the charge cycle.

Cobalt exhibited a lower E_{max} after 600 cycles compared to nickel in the GCD analysis due to several intrinsic and structural factors that affect their performance as electrode materials. Cobalt tends to undergo more significant changes in oxidation states during electrochemical reactions, which can lead to structural degradation. This instability is primarily due to the formation of Co(III) and Co(IV) species, which can be less stable than the oxidation states commonly found in nickel. Furthermore, the redox behavior of cobalt compounds, such as cobalt oxyhydroxide (CoOOH), is often less reversible than that of nickel compounds. For instance, studies show that CoOOH formed through different methods exhibits varied stability, with some forms demonstrating poor capacity

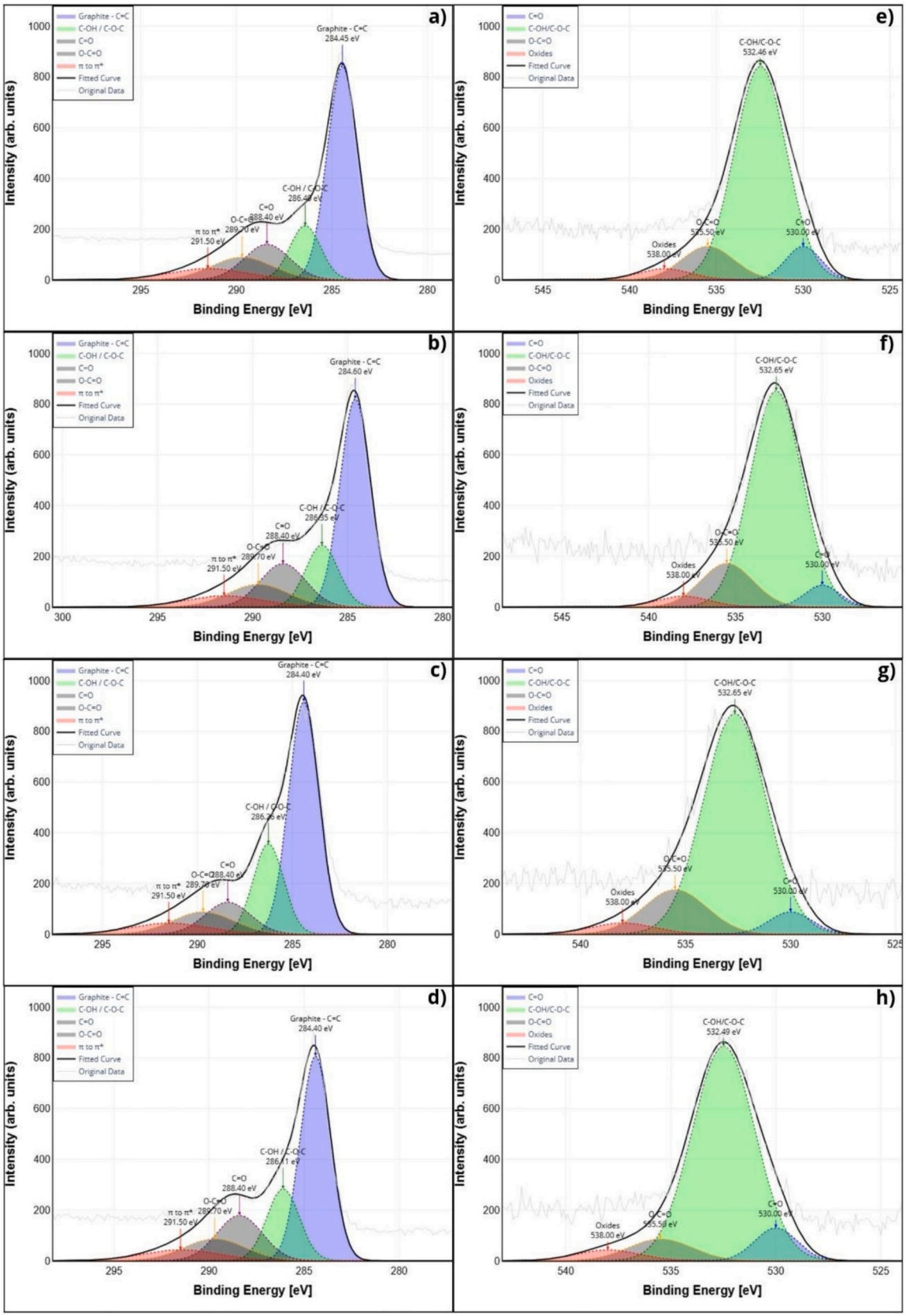

Fig. 4. High-resolution XPS spectra of C 1s: a) AC-S, b) AC-S2%Co, c) AC-S2%Cu and d) AC-S2%Ni; and XPS spectra of O 1s: e) AC-S, f) AC-S2%Co, g) AC-S2%Cu and h) AC-S2%Ni.

Table 3
Specific capacitance values for each sample.

Sample	Curve area (C.g^{-1})	Specific Capacitance (F.g^{-1})[a]
AC-S	4.52	37.71
AC-S2%Co	3.53	29.40
AC-S2%Cu	3.66	30.47
AC-S2%Ni	7.15	59.58

[a] At scan rate of 100 mV.s^{-1}.

retention under cycling conditions. In contrast, nickel compounds generally maintain better redox reversibility, contributing to improved cyclic stability [36,44].

The conditions under which electrochemical tests are conducted (such as pH and electrolyte composition) can also influence the cyclic stability of electrode materials. Nickel typically performs better across a wider range of conditions, maintaining its structural integrity and electrochemical activity longer than cobalt [44,45]. Regarding cyclic capacitance retention, all samples demonstrated good stability at 700 cycles. There is a drop in this retention during the first 100 cycles, which is characteristic of the formation of the interface between the electrolyte and the electrode. Between 100 and 700 cycles, AC-S demonstrated 89 %, AC-S2%Cu demonstrated 93 %, AC-S2%Co demonstrated 99 %, and AC-S2%Ni demonstrated 98 % of specific capacitance retention, respectively.

Energy density in supercapacitors can be improved with redox-active electrode materials, either by decoration or composite fabrication [46]. Table 5 contains values for energy density and power density of the

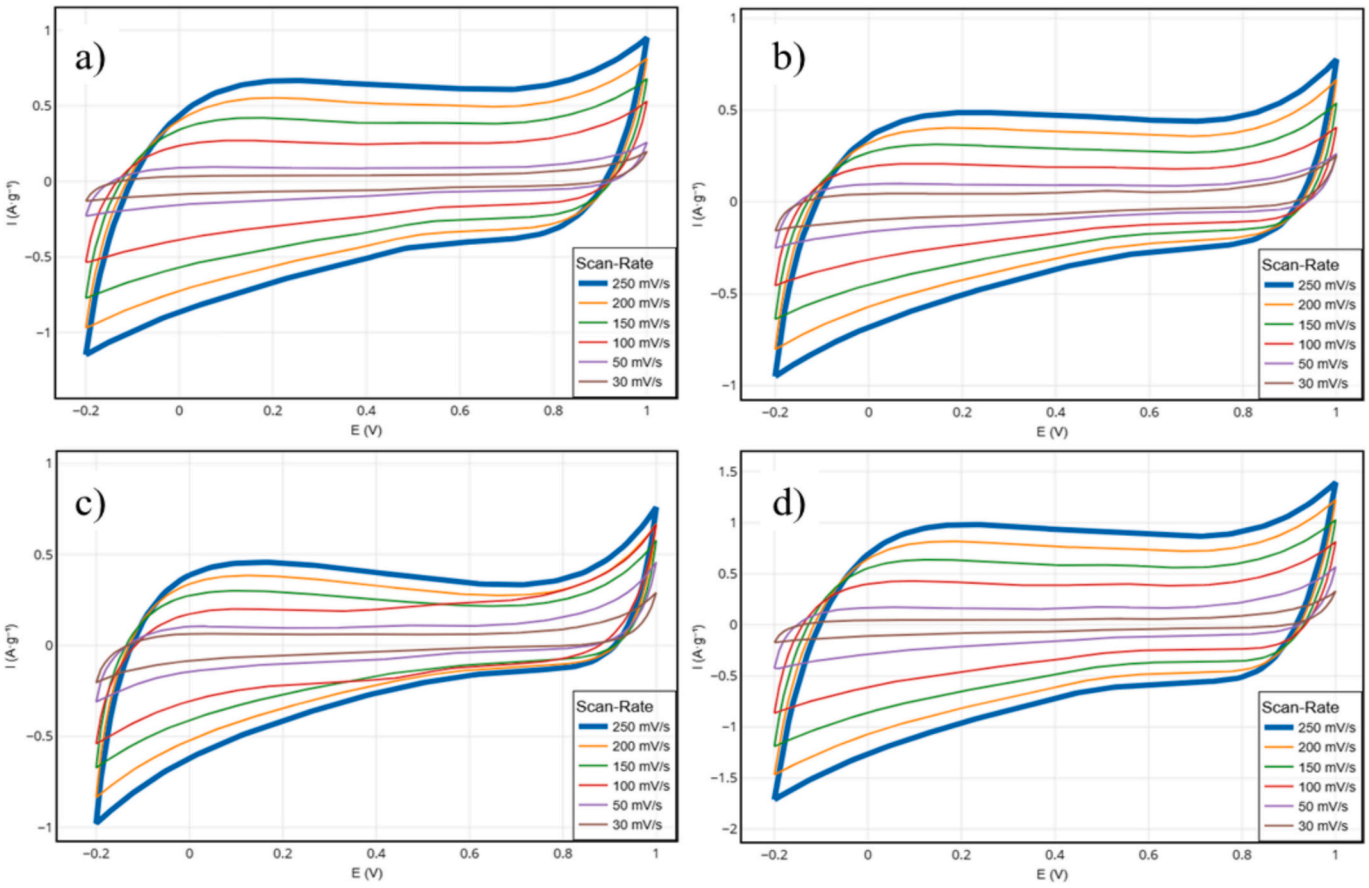

Fig. 5. Cyclic voltammetry graphs performed at a multiple range scan rate for all elements a) AC-S, b) AC-S2%Co, c) AC-S2%Cu and d) AC-S2%Ni.

Table 4
Specific capacitance and energy density for different electrodes.

Material type	Method	Activating Agent	Specific Capacitance (F. g^{-1})	Energy Density (Wh. kg^{-1})	Ref.
Ni modified commercial activated carbon	Chemical activation	H_2SO_4	59.58	93.73	This work
Bamboo-based ACs	Carbonization followed by chemical activation	HCl	9.0	–	[38]
Jute sticks	Chemical activation & pyrolysis	$NaHCO_3$	150.0	20	[39]
Commercial activated carbon	–	–	29.0	–	
Copper nanocrystal modified activated carbon	Chemical activation & heat treating in N_2	HNO_3	78.0	34.7	[40]
Commercial activated carbon	chemical activation	H_3PO_4	249.0	–	[41]
Nickel-oxide/activated carbon composites	Hydrothermal process and pyrolyzed	–	364.13	44.07	[42]
Waste sugarcane bagasse-derived activated carbon	Pyrolyzed anc chemical ativation	KOH	282.25	43.26	[43]
N,P-doped activated carbons from chitosan	Chemical activation & pyrolysis	H_3PO_4	24	18.2	[7]

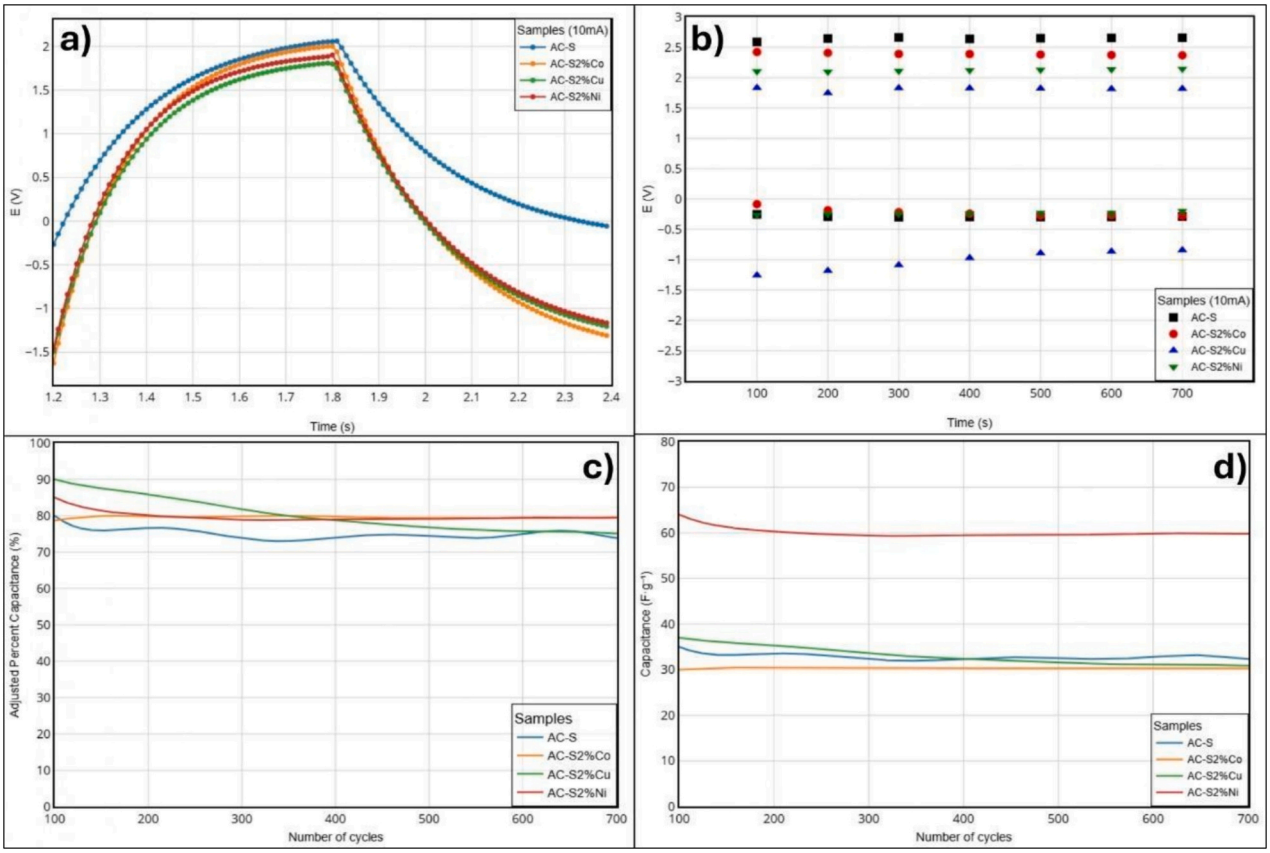

Fig. 6. Charge-discharge curves of the electrodes at 10 mA.g^{-1} - (a) a representative charge and discharge cycle, (b) E_{max} over 600 cycles, (c) Cyclic Capacitance retention and (d) Specific Capacitance Retention.

samples. It is possible to observe that electrodes containing metals are capable of delivering greater power over a wider voltage range. The energy and power density values are consistent with the specific capacitance values found, with AC-S2%Ni being the sample that exhibited the highest E and *P* values, 93.73 (Wh·kg^{-1}) and 4938 (W·kg^{-1}) respectively. From the data in Table 4, it can be observed that the E value demonstrated by AC-S2%Ni is promising even though the specific capacitance value is lower than in other studies using activated carbon electrodes containing nickel. While capacitance is fundamental, higher energy and power densities are superior metrics because they directly translate to how much energy a supercapacitor can store and how quickly it can deliver it [47,48].

3.4.3. *Electrochemical impedance spectroscopy*

EIS measurements were used to investigate the electrochemical behavior of the supercapacitor at the electrode/electrolyte interface. The Nyquist plots were used to illustrate the electrochemical impedance of the electrodes (Fig. 7). The impedance behavior of the electrodes is close to ideal electrochemical capacitance behavior with a small semicircle at high frequency region and nearly vertical lines at the low frequency region. AC-S and AC-S2%Co presented similar behavior, with a wide semicircle. AC-S2%Ni sample presented the format closest to the ideal, as also reported by [49], with a smaller semicircle, indicating good capacitive behavior. However, the Warburg slope is smaller than the others, representing a certain diffusional resistance. AC-S2%Cu demonstrated a more resistive behavior with ESR at approximately 40 Ω. The greater resistance of AC-S2%Cu may be associated with lower wettability by the electrolyte, as can be seen below.

Table 5
Energy and power density for the studied samples.

Sample	Voltage (V)	E (Wh.kg^{-1})	P (W.kg^{-1})
AC-S	2.387	29.76	2244
AC-S2%Co	3.864	60.79	2831
AC-S2%Cu	3.390	48.49	2574
AC-S2%Ni	3.416	93.73	4938

3.5. *Surface wettability*

The wettability of an electrode by an electrolyte is a critical factor in the performance of supercapacitors. Wettability affects the interface between the electrode and the electrolyte, which is crucial for charge storage. Good wettability ensures that the electrolyte can penetrate the electrode's porous structure, facilitating ion transport and enhancing the electrochemical reactions necessary for charge storage. High wettability promotes better ionic transport within the electrode material. When an electrode is well-wetted, ions from the electrolyte can easily access the active sites on the electrode surface, leading to faster charge/discharge rates. This is particularly important for supercapacitors, which rely on rapid ion movement to achieve high power density. Furthermore, enhanced wettability can lead to improved capacitance values due to more effective utilization of the electrode surface area [32].

It is known that there is a relationship between a better electrochemical response of the electrode and a smaller contact angle with water for aqueous electrolytes. This can be corroborated by evaluating the data obtained in Table 5, where AC-Ni presents the lowest contact angle value and consequently the best capacitance and specific capacitance when compared to other metals and commercial activated carbon. In this study, it was found that the activated carbon electrode treated with sulfuric acid presented greater wettability, lower than the value obtained by Li et al. [3] which was 129.7° for activated carbon, as can be seen in Table 6. This may be due to a greater surface interaction between

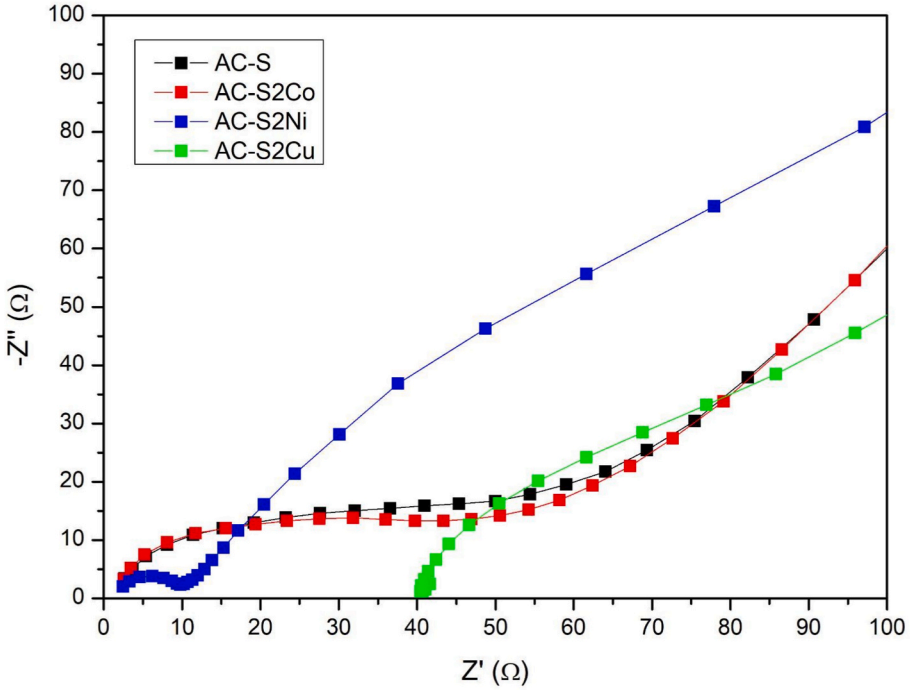

Fig. 7. Impedance spectra for hybrid-activated carbon electrodes.

the sulfate electrolyte and the possible sulfur atoms present on the surface of the treated activated carbon.

4. Conclusions

This study evaluated the surface modification of commercial activated carbon through sulfuric acid treatment and metal deposition via magnetron sputtering, aiming to improve its performance as an electrode material for energy storage applications. The results demonstrated that these combined strategies are effective in enhancing the physicochemical and electrochemical properties of the carbon structure. Acid treatment led to a substantial increase in specific surface area, from 562 $m^2 \cdot g^{-1}$ to 1048 $m^2 \cdot g^{-1}$, and promoted the formation of mesopores, which are essential for improving electrolyte accessibility and facilitating ion transport. These structural improvements directly contributed to increased capacitance. Metal deposition with cobalt (Co), copper (Cu), and nickel (Ni) further modified the morphology and surface chemistry of the material. XPS analysis revealed an increase in the fraction of graphitic carbon, which enhances electrical conductivity, while oxygenated functional groups—responsible for pseudocapacitive behavior—were maintained at optimized levels. The sample modified with 2 wt% Ni achieved the highest specific capacitance (59.58 $F \cdot g^{-1}$ at 100 $mV \cdot s^{-1}$), showing a good balance between electrical conductivity and redox activity. Electrochemical characterization through cyclic voltammetry and galvanostatic charge–discharge confirmed the stability and efficiency of the metal-modified electrodes. While the Ni-based electrode stood out in capacitance, the Co- and Cu-based materials achieved higher power densities, reflecting their ability to operate in wider potential windows. In addition to electrochemical performance, surface area and porosity also varied depending on the treatment method. For instance, the Ni-decorated sample reached a BET surface area of 1984 $m^2 \cdot g^{-1}$, far exceeding the ~500 $m^2 \cdot g^{-1}$ typically reported for untreated commercial AC. This surface enhancement, combined with improved wettability (as evidenced by lower contact angle values), favors efficient charge storage even at low metal content. A strong correlation was observed between electrode wettability and electrochemical performance, emphasizing the importance of surface interaction in aqueous electrolytes. These findings reinforce that surface modification—both chemical and physical—is a key factor in tuning the properties of carbon-based electrodes to optimize their performance.

While the results are promising, some limitations must be acknowledged. One potential trade-off is that, although sputtering produces uniform coatings, excessive metal deposition may lead to partial pore blockage, reducing the accessible surface area and hindering ion diffusion. This effect was mitigated in this study by limiting the deposition time, but it remains a critical parameter for optimization. Furthermore, although magnetron sputtering is a clean and controllable process, its industrial scalability may be constrained by equipment costs and throughput. In terms of sustainability, the sulfuric acid treatment employed is relatively mild, but still generates acidic effluents that require appropriate handling to minimize environmental impact. In

Table 6
Water contact angle and representative images of the WCA analysis at time zero of the samples.

Sample	Water contact angle	
AC-S	122.1° ± 6.2	
AC-S2%Co	120.9° ± 5.6	
AC-S2%Cu	125.3° ± 2.3	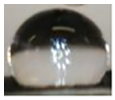
AC-S2%Ni	115.4° ± 3.5	

summary, this work confirms that combining mild chemical activation with solvent-free metal deposition is a viable and effective strategy to enhance the electrochemical properties of activated carbon for supercapacitor applications. The materials developed here exhibit competitive performance while offering advantages in process simplicity and environmental safety. Future studies should focus on optimizing deposition parameters, exploring greener activation alternatives, and evaluating long-term cycling stability in real-world operating conditions. These advances will help bring metal-doped carbon electrodes closer to practical use in next-generation energy storage technologies. Future research should explore the use of alternative carbon precursors derived from renewable biomass sources, which may offer tunable porosity and reduced environmental impact. In addition, advanced activation methods—such as physical activation with CO_2 or steam, or green chemical agents—could further improve surface functionality and sustainability. The optimization of sputtering parameters for various metals and oxide phases, as well as the integration of additional redox-active species (e.g., conducting polymers or metal oxides), may further enhance electrochemical performance. Hybrid devices that combine EDLC and pseudocapacitive mechanisms, or pair AC-based electrodes with batteries or fuel cells, also represent a promising direction for expanding the applicability of these materials in next-generation energy storage systems. Long-term cycling stability, mechanical robustness, and performance in full-cell configurations should also be addressed to validate their practical potential for commercial deployment.

Data and code availability

Data are contained within the article.

CRediT authorship contribution statement

Andrielen Braz Vanzetto: Writing – original draft, Visualization, Investigation, Formal analysis, Data curation, Conceptualization. **Francisco Teloken:** Visualization, Formal analysis, Data curation. **Mateus Beltrami:** Investigation, Formal analysis, Data curation. **Lidia Kunz Lazzari:** Validation, Data curation, Conceptualization. **Heitor Luiz Ornaghi Júnior:** Writing – review & editing, Visualization, Validation. **Matheus Poletto:** Writing – review & editing, Validation. **Otávio Titton Dias:** Writing – review & editing, Validation, Supervision. **Ademir José Zattera:** Validation, Supervision, Funding acquisition.

Ethical approval

Not Applicable.

Declaration of competing interest

The authors declare the following financial interests/personal relationships which may be considered as potential competing interests:

Andrielen Braz VAnzetto reports financial support was provided by National Council for Scientific and Technological Development. Francisco TEloken reports was provided by Coordination of Higher Education Personnel Improvement. If there are other authors, they declare that they have no known competing financial interests or personal relationships that could have appeared to influence the work reported in this paper.

Acknowledgments

The authors would like to thank CNPq and CAPES for the financial support, the Postgraduate Program in Process and Technology Engineering (PGEPROTEC) and the University of Caxias do Sul (UCS) for the academic support during this research.

Appendix A. Supplementary data

Supplementary data to this article can be found online at https://doi.org/10.1016/j.diamond.2025.112688.

Data availability

Data will be made available on request.

References

[1] Z. Kudaş, M.A. Kabala, D. Ekinci, Electrochemical synthesis and characterization of titanium oxide thin films on covalent polyphenylene-modified gold electrodes as electrode materials for supercapacitor applications, J. Electroanal. Chem. 978 (2025), https://doi.org/10.1016/j.jelechem.2024.118896.
[2] R.Y. N, K. Sharma, P.M. Shafi, An overview, methods of synthesis and modification of carbon-based electrodes for supercapacitor, J Energy Storage 55 (2022) 105727, https://doi.org/10.1016/j.est.2022.105727.
[3] Y. Li, X. Fan, M. Zhang, L. Cui, T. Jiao, Enhanced electrochemical performance of the activated carbon electrodes with a facile and in-situ phosphoric acid modification, J Energy Storage 24 (2019) 100744, https://doi.org/10.1016/j.est.2019.04.018.
[4] X. Zhang, Z. Qiu, Q. Li, L. Liang, X. Yang, S. Lu, D. Xiang, F. Lai, Nickel acetate-assisted graphitization of porous activated carbon at low temperature for supercapacitors with high performances, Front. Chem. 10 (2022) 1–7, https://doi.org/10.3389/fchem.2022.828381.
[5] S.M. Yakout, G. Sharaf El-Deen, Characterization of activated carbon prepared by phosphoric acid activation of olive stones, Arab. J. Chem. 9 (2016) S1155–S1162, https://doi.org/10.1016/j.arabjc.2011.12.002.
[6] S. Ullah, S.S.A. Shah, M. Altaf, I. Hossain, M.E. El Sayed, M. Kallel, Z.M. El-Bahy, A. ur Rehman, T. Najam, M.A. Nazir, Activated carbon derived from biomass for wastewater treatment: synthesis, application and future challenges, J. Anal. Appl. Pyrolysis 179 (2024) 106480, https://doi.org/10.1016/j.jaap.2024.106480.
[7] Emerson Vega-Ramírez, et al., Sustainable synthesis of N, P-doped activated carbons from chitosan for superior supercapacitor performance, Electrochim. Acta (2025) 146405, https://doi.org/10.1016/j.electacta.2025.146405.
[8] Rashed Ali Mohamed Adam, et al., Electropolymerization of polyaniline on coated activated carbon derived from human hair as a bilayer electrode for supercapacitor applications, J Energy Storage 129 (2025) 117356, https://doi.org/10.1016/j.est.2025.117356.
[9] Sadegh Azizi, Mohammad Bagher Askari, Parisa Salarizadeh, ZnS/FeS/activated carbon derived from rice husk loaded on nickel foam as a novel electrode material for supercapacitors, Diam. Relat. Mater. (2025) 112459, https://doi.org/10.1016/j.diamond.2025.112459.
[10] Hongbo Xu, et al., Low-cost synthesis of sulfur doped apricot shell activated carbon material with hierarchical porous structure for flexible supercapacitor, Mater. Sci. Eng. B 320 (2025) 118428, https://doi.org/10.1016/j.mseb.2025.118428.
[11] Hasan Sayğılı, Gülbahar Akkaya Sayğılı, Abdulkadir Levent, Design of microwave-supported activated carbon derived from lentil processing residual for efficient heavy metals adsorption and supercapacitor applications, Talanta 293 (2025) 128068, https://doi.org/10.1016/j.talanta.2025.128068.
[12] F. Markoulidis, C. Trapalis, N. Todorova, R. Grilli, C. Lekakou, Composite electrodes of activated carbon and multiwall carbon nanotubes decorated with silver nanoparticles for high power energy storage, J. Compos. Sci. 3 (2019), https://doi.org/10.3390/jcs3040097.
[13] J. Pan, C. Li, Y. Peng, L. Wang, B. Li, G. Zheng, M. Song, Application of transition metal (Ni, Co and Zn) oxides based electrode materials for ion-batteries and supercapacitors, Int. J. Electrochem. Sci. 18 (2023) 100233, https://doi.org/10.1016/j.ijoes.2023.100233.
[14] A.S. Winata, H. Devianto, R.F. Susanti, Synthesis of activated carbon from salacca peel with hydrothermal carbonization for supercapacitor application, Mater. Today Proc. 44 (2021) 3268–3272, https://doi.org/10.1016/j.matpr.2020.11.515.
[15] J. Pan, C. Li, Y. Peng, L. Wang, B. Li, G. Zheng, M. Song, Application of transition metal (Ni, co and Zn) oxides based electrode materials for ion-batteries and supercapacitors, Int. J. Electrochem. Sci. 18 (2023) 100233, https://doi.org/10.1016/j.ijoes.2023.100233.
[16] Y. Liu, X. Xu, Z. Shao, S.P. Jiang, Metal-organic frameworks derived porous carbon, metal oxides and metal sulfides-based compounds for supercapacitors application, Energy Storage Mater. 26 (2020) 1–22, https://doi.org/10.1016/j.ensm.2019.12.019.
[17] S. Mandal, J. Hu, S.Q. Shi, A comprehensive review of hybrid supercapacitor from transition metal and industrial crop based activated carbon for energy storage applications, Mater. Today Commun. 34 (2023) 105207, https://doi.org/10.1016/j.mtcomm.2022.105207.
[18] R. Garg, S. Gonuguntla, S. Sk, M.S. Iqbal, A.O. Dada, U. Pal, M. Ahmadipour, Sputtering thin films: materials, applications, challenges and future directions, Adv. Colloid Interf. Sci. 330 (2024) 103203, https://doi.org/10.1016/j.cis.2024.103203.
[19] N. Tanapongpisit, S. Wongprasod, P. Laohana, S. Sonsupap, J. Khajonrit, S. Musikajaroen, U. Wongpratat, B. Yotburut, S. Maensiri, W. Meevasana, W. Saenrang, Enhancing activated carbon supercapacitor electrodes using sputtered Cu-doped BiFeO3 thin films, Sci. Rep. 14 (2024) 1–11, https://doi.org/10.1038/s41598-024-79439-3.

[20] L. Zhang, S.L. Candelaria, J. Tian, Y. Li, Y.X. Huang, G. Cao, Copper nanocrystal modified activated carbon for supercapacitors with enhanced volumetric energy and power density, J. Power Sources 236 (2013) 215–223, https://doi.org/10.1016/j.jpowsour.2013.02.036.
[21] Z. Heidarinejad, M.H. Dehghani, M. Heidari, G. Javedan, I. Ali, M. Sillanpää, Methods for preparation and activation of activated carbon: a review, Environ. Chem. Lett. 18 (2020) 393–415, https://doi.org/10.1007/s10311-019-00955-0.
[22] L.F. Sosa, M.A.S. Garcia, A.C.A. Silva, B.S. Archanjo, A.F. Feil, D. Eberhardt, S.J. A. Figueroa, J.M.A.R. de Almeida, P.N. Romano, Highly efficient low metal content Ni/CeO2 catalysts prepared by magnetron sputtering deposition for ethanol steam reforming reaction, Appl. Catal. B Environ. 365 (2025), https://doi.org/10.1016/j.apcatb.2024.124940.
[23] T.J. Patey, A. Hintennach, F. La Mantia, P. Novák, Electrode engineering of nanoparticles for lithium-ion batteries-role of dispersion technique, J. Power Sources 189 (2009) 590–593, https://doi.org/10.1016/j.jpowsour.2008.09.091.
[24] S. Zhang, M. Zheng, Y. Tang, R. Zang, X. Zhang, X. Huang, H. Pang, Understanding synthesis–structure–performance correlations of nanoarchitectured activated carbons for electrochemical applications and carbon capture, Adv. Funct. Mater. 32 (40) (2022) 2204714, https://doi.org/10.1002/adfm.202204714.
[25] Z. Abdelouahab-Reddam, A. Wahby, R. El Mail, J. Silvestre-Albero, F. Rodríguez-Reinoso, A. Sepúlveda-Escribano, Activated carbons impregnated with Na2S and H2SO 4: texture, surface chemistry and application to mercury removal from aqueous solutions, Adsorpt. Sci. Technol. 32 (2014) 101–115, https://doi.org/10.1260/0263-6174.32.2-3.101.
[26] İ. Demiral, C. Samdan, H. Demiral, Enrichment of the surface functional groups of activated carbon by modification method, Surf. Interfaces 22 (2021), https://doi.org/10.1016/j.surfin.2020.100873.
[27] Z. Teimouri, S. Nanda, N. Abatzoglou, A.K. Dalai, Application of activated carbon in renewable energy conversion and storage systems: a review, Environ. Chem. Lett. 22 (2024) 1073–1092, https://doi.org/10.1007/s10311-023-01690-3.
[28] B. Sukhbaatar, W. Qing, J. Seo, S. Yoon, B. Yoo, Uniformly dispersed ruthenium nanoparticles on porous carbon from coffee waste outperform platinum for hydrogen evolution reaction in alkaline media, Sci. Rep. 14 (2024) 1–9, https://doi.org/10.1038/s41598-024-56510-7.
[29] J.H. Han, H.W. Kang, W. Lee, Highly porous and capacitive copper oxide nanowire/graphene hybrid carbon nanostructure for high-performance supercapacitor electrodes, Compos. Part B Eng. 178 (2019) 107464, https://doi.org/10.1016/j.compositesb.2019.107464.
[30] T. Weiss, V. Zielasek, M. Bäumer, Influence of water on chemical vapor deposition of Ni and co thin films from ethanol solutions of acetylacetonate precursors, Sci. Rep. 5 (2015) 18194, https://doi.org/10.1038/srep18194.
[31] A.M. Puziy, O.I. Poddubnaya, R.P. Socha, J. Gurgul, M. Wisniewski, XPS and NMR studies of phosphoric acid activated carbons, Carbon 46 (2008) 2113–2123, https://doi.org/10.1016/j.carbon.2008.09.010.
[32] L. Zhao, Y. Li, M. Yu, Y. Peng, F. Ran, Electrolyte-wettability issues and challenges of electrode materials in electrochemical energy storage, energy conversion, and beyond, Adv. Sci. 10 (2023), https://doi.org/10.1002/advs.202300283.
[33] A.A. Kumar, V.D. Kumar, E. Berdimurodov, Recent trends in noble-metals based composite materials for supercapacitors: a comprehensive and development review, J. Indian Chem. Soc. 100 (2023) 100817, https://doi.org/10.1016/j.jics.2022.100817.
[34] W.G. Nunes, A.N. Miranda, B. Freitas, R. Vicentini, A.C. Oliveira, G. Doubek, R. G. Freitas, L.M. Da Silva, H. Zanin, Charge-storage mechanism of highly defective NiO nanostructures on carbon nanofibers in electrochemical supercapacitors, Nanoscale 13 (2021) 9590–9605, https://doi.org/10.1039/d1nr00065a.
[35] R. Yadav, N. Macherla, K. Singh, K. Kumari, Synthesis and electrochemical characterization of activated porous carbon derived from walnut shells as an electrode material for symmetric supercapacitor application †, Eng. Proc. 59 (2023) 1–8, https://doi.org/10.3390/engproc2023059175.
[36] L. Zhang, S.L. Candelaria, J. Tian, Y. Li, Y.X. Huang, G. Cao, Copper nanocrystal modified activated carbon for supercapacitors with enhanced volumetric energy and power density, J. Power Sources 236 (2013) 215–223, https://doi.org/10.1016/j.jpowsour.2013.02.036.
[37] R. Li, X. Liu, H. Wang, Y. Wu, Z.P. Lu, Development of electrochemical supercapacitors with uniform nanoporous silver network, Electrochim. Acta 182 (2015) 224, https://doi.org/10.1016/j.electacta.2015.09.069.
[38] Chan Kim, et al., Feasibility of bamboo-based activated carbons for an electrochemical supercapacitor electrode, Korean J. Chem. Eng. 23 (2006) 592–594, https://doi.org/10.1007/BF02706799.
[39] Syed Shaheen Shah, et al., Jute sticks derived and commercially available activated carbons for symmetric supercapacitors with bio-electrolyte: a comparative study, Synth. Met. 277 (2021) 116765, https://doi.org/10.1016/j.synthmet.2021.116765.
[40] Lili Zhang, et al., Copper nanocrystal modified activated carbon for supercapacitors with enhanced volumetric energy and power density, J. Power Sources 236 (2013) 215–223, https://doi.org/10.1016/j.jpowsour.2013.02.036.
[41] Yonggang Li, et al., Enhanced electrochemical performance of the activated carbon electrodes with a facile and in-situ phosphoric acid modification, J Energy Storage 24 (2019) 100744, https://doi.org/10.1016/j.est.2019.04.018.
[42] Jyoti Singh, et al., Preparation of nickel oxide nanoparticles/biomass-derived activated carbon composites for high-performance aqueous asymmetric supercapacitor electrode, Surf. Interfaces 56 (2025) 105736, https://doi.org/10.1016/j.surfin.2024.105736.
[43] Jyoti Singh, et al., Facile fabrication of sulfur-doped porous carbon from waste sugarcane bagasse for high performance supercapacitors, Diam. Relat. Mater. 149 (2024) 111640, https://doi.org/10.1016/j.diamond.2024.111640.
[44] B.M. Pires, W.G. Nunes, B.G. Freitas, F.E.R. Oliveira, V. Katic, C.B. Rodella, L.M. Da Silva, H. Zanin, Characterization of porous cobalt hexacyanoferrate and activated carbon electrodes under dynamic polarization conditions in a sodium-ion pseudocapacitor, J. Energy Chem. 54 (2020) 53–62.
[45] S.-K. Chang, Z. Zainal, K.-B. Tan, N.A. Yusof, W.M.D.W. Yusoff, S.R.S. Prabaharan, Synthesis and electrochemical properties of nanostructured nickel–cobalt oxides as supercapacitor electrodes in aqueous media, Int. J. Energy Res. 39 (2015) 1366–1377, https://doi.org/10.1002/er.3339.
[46] M. Karnan, A.G.K. Raj, K. Subramani, S. Santhoshkumar, M. Sathish, The fascinating supercapacitive performance of activated carbon electrodes with enhanced energy density in multifarious electrolytes, sustain, Energy Fuel 4 (2020) 3029–3041, https://doi.org/10.1039/c9se01298b.
[47] YanLei Zhang, Chen Sun, ZhiShu Tang, High specific capacitance and high energy density supercapacitor electrodes enabled by porous carbon with multilevel pores and self-doped heteroatoms derived from Chinese date, Diam. Relat. Mater. 97 (2019) 107455, https://doi.org/10.1016/j.diamond.2019.107455.
[48] M.D. Merrill, et al., Optimizing supercapacitor electrode density: achieving the energy of organic electrolytes with the power of aqueous electrolytes, RSC Adv. 4 (81) (2014) 42942–42946, https://doi.org/10.1039/C4RA08114E.
[49] A.M. Abioye, Z.A. Noorden, F.N. Ani, Synthesis and characterizations of electroless oil palm shell based-activated carbon/nickel oxide nanocomposite electrodes for supercapacitor applications, Electrochim. Acta 225 (2017) 493–502.